Highly Emissive and Color-Tunable $CuInS_2$-Based Colloidal Semiconductor Nanocrystals: Off-Stoichiometry Effects and Improved Electroluminescence Performance

Bingkun Chen, Haizheng Zhong, Wenqing Zhang, Zhan'ao Tan,* Yongfang Li, Cairan Yu, Tianyou Zhai, Yoshio Bando, Shengyi Yang, and Bingsuo Zou*

The off-stoichiometry effects and gram-scale production of luminescent $CuInS_2$-based semiconductor nanocrystals, as well as their application in electroluminescence devices are reported. The crystal structures and optical properties of $CuInS_2$ nanocrystals can be significantly influenced by controlling their [Cu]/[In] molar ratio. A simple model adapted from the bulk materials is proposed to explain their off-stoichiometry effects. Highly emissive and color-tunable $CuInS_2$-based NCs are prepared by a combination of [Cu]/[In] molar ratio optimization, ZnS shell coating, and $CuInS_2$–ZnS alloying. The method is simple, hassle-free, and easily scalable to fabricate tens of grams of nanocrystal powders with photoluminescence quantum yields up to around 65%. Furthermore, the performance of high-quality $CuInS_2$-based NCs in electroluminescence devices is examined. These devices have lower turn-on voltages of around 5 V, brighter luminance up to approximately 2100 cd m^{-2} and improved injection efficiency of around 0.3 lm W^{-1} (at 100 cd m^{-2}) in comparison to recent reports.

1. Introduction

Colloidal semiconductor nanocrystals (NCs) have received considerable attention because of their interesting optical properties[1] and potential applications as light-emitting and solar-harvesting materials.[2–8] As new generation light-emitting materials, semiconductor NCs have size-tunable emissions due to quantum size effects; they also exhibit a high resistance toward photobleaching.[9] Study of their properties and exploration of potential applications demand large amounts of high-quality NCs with tunable and superior emissive properties. Previous works on highly emissive and color-tunable NCs mainly focus on toxic materials containing cadmium or lead.[10] I–III–VI semiconductor NCs, including $CuInS_2$, have low toxicity, tunable emissions in the wavelengths of the visible to near infrared region, high absorption coefficients, large Stokes shifts, and high emission intensities.[11–23] They are considered to be alternative low-toxicity materials for bio-imaging and solid-state lighting,[17,18] as well as suitable candidates to act as solar harvesters for solution process solar cell devices.[19,20] Therefore, synthesis of high-quality $CuInS_2$-based NCs is of great interest.

The synthetic chemistry of $CuInS_2$ NCs has been extensively studied, based on approaches including precursor thermal decomposition,[12–14] hot-injection methods,[15–17,20] hydrothermal methods,[24,25] and microwave assisted methods.[26] To improve their photoluminescence (PL) emission properties, shell coating and alloying strategies have been adapted to produce high quality I–III–VI NCs.[27–35] Literature reports and our previous results have revealed that stoichiometry control is very important in the production of highly luminescent $CuInS_2$ NCs.[13,14,27–35] In addition, $CuInS_2$ NCs have the characteristic of long PL lifetime, which was thought to be related to intrinsic defects.[36] Based on theoretical models and experimental works on bulk materials, the intrinsic defects of I–III–VI $CuInS_2$ and $CuInSe_2$ materials have been found to be related to off-stoichiometry effects.[37,38] Although stoichiometry

B. Chen, Prof. H. Zhong, Prof. S. Yang, Prof. B. Zou
School of Materials Science & Engineering
Micro/Nano Research Center
Beijing Institute of Technology
5 Zhongguancun South Street, Beijing 100081, China
E-mail: hzzhong@bit.edu.cn
W. Zhang, Prof. Z. Tan
State Key Laboratory of Alternate Electrical Power System with Renewable Energy Sources
The New and Renewable Energy of Beijing Key Laboratory
North China Electric Power University
Beijing 102206, China
E-mail: tanzhanao@ncepu.edu.cn
Prof. Y. Li
CAS Key Laboratory of Organic Solids
Institute of Chemistry
Chinese Academy of Sciences
Beijing 100190, China
Dr. C. Yu
CAS Key Lab of Photochemistry
Institute of Chemistry
Chinese Academy of Sciences
Beijing 100190, China
Dr. T. Zhai, Prof. Y. Bando
International Center for Materials Nanoarchitectonics (MANA)
National Institute for Materials Science (NIMS)
Namiki 1-1, Tsukuba, Ibaraki 305-0044, Japan

DOI: 10.1002/adfm.201102496

control of $CuInS_2$ NCs has been reported,[39] it is still of great interest to further understand off-stoichiometry effects on the physical properties of $CuInS_2$ NCs.

The applications of luminescent NCs in electroluminescence (EL) devices has offered quantum dot-based LEDs (QD-LEDs) as new generation solid-state-lighting and display technologies, which possess advantages over competing device types, including low cost, superior color tunability, large area, and compatible with various substrates.[40–42] High-quality NCs are necessary to achieve better device performance. QD-LEDs in previous reports are mainly based on CdSe NCs.[43–45] Very recently, I–III–VI NCs have appeared as cadmium-free active layers in QD-LEDs.[34,46,47] EL emissions ranging from green to NIR as well as white light emissions were observed in light-emitting devices using ZnCuInS/ZnSe/ZnS or $CuInSe_2$/ZnS NCs as emitting materials.[34,46,47] I–III–VI NCs also have the potential to be light down-converters for white LEDs.[33,48] This research is at an early stage and improvements in efficiency and reliability are greatly aspired to; a comprehensive exploration of I–III–VI NCs in light-emitting applications requires large amounts (at least grams) of high-quality (high PL QYs) NCs.

We recently reported a facile route to synthesize high-quality $CuInS_2$ NCs at the gram scale by using CuI, $In(OAc)_3$, and 1-dodecanethiol as precursors.[13,14] In this work, we control the [Cu]/[In] molar ratio of colloidal $CuInS_2$ NCs by varying the ratio of copper and indium reagents. The off-stoichiometry effects on crystal structure and optical properties of $CuInS_2$ NCs are observed and discussed. The mechanism underlying the stoichiometry-dependence of PL properties is discussed and the PL emission properties optimized by choosing a suitable [Cu]/[In] molar ratio. We further apply ZnS shell coating and $CuInS_2$–ZnS alloying strategies to prepare high emissive and color-tunable I–III–VI NCs. We also examine the performance of as-prepared NCs in EL devices. The performance of light-emitting devices is much better than Tan's recent report[47] and among the best for non-cadmium materials.[49,50]

2. Results and Discussion

Ternary I–III–VI compounds with chalcopyrite structure (tetragonal phase) are viewed as derived materials of II–VI zinc-blende binary analogs. (For example, $Zn_{0.5}Cd_{0.5}S$ is the binary analog for $CuInS_2$).[37,51–54] Unlike their II–VI binary analogs, I–III–VI compounds can tolerate a large range of anion and cation off-stoichiometry, which gives them the ability to induce different doping defects. Either p- or n-type $CuInS_2$ and $CuInSe_2$ materials can be produced via stoichiometry control.[37] This provides an effective route to tune their electronic properties for high-efficiency photovoltaic cells. For I–III–VI NCs, crystal defects determine their PL emissions.[34,39] The intrinsic off-stoichiometry effects of I–III–VI compounds may provide a route to optimize their PL properties. An earlier report by Maeda *et al.* observed an off-stoichiometry effect on PL emissions in $CuInS_2$ NCs that were synthesized through a hot-injection method.[39] By tuning their [Cu]/[In] ratio, the PL emissions of $CuInS_2$ NCs can be greatly enhanced. This work focuses on the off-stoichiometry effects on the crystal structures and optical properties of $CuInS_2$ NCs.

The amounts of elements offered for chemical reaction govern the resulting stoichiometry. We achieved composition control of the $CuInS_2$ NCs by varying the molar ratio of CuI and $In(OAc)_3$ precursors. The resulting samples were collected and purified following the method described in the Experimental Section. Energy dispersive X-ray (EDX) spectra were performed to quantitatively analyze the composition of these samples. A typical EDX spectrum is shown in Figure S1 and the chemical compositions of $CuInS_2$ NCs are summarized in Table S1 (Supporting Information). By tuning the weight ratio of CuI and $In(OAc)_3$ precursors, the [Cu]/[In] molar ratio of the resulting NCs was gradually changed from 0.3 to 2.9. The off-stoichiometry range in $CuInS_2$ NCs is much larger than that of observations in bulk materials and Maeda's report.[37,39] According to Zunger's theory of I–III–VI bulk materials, the larger off-stoichiometry for Cu-poor $CuInS_2$ NCs can be explained by the easy formation of copper vacancies and the existence of defect pairs of copper vacancies and In on Cu antisites ($2V_{Cu}^{-} + In_{Cu}^{2+}$) pairs.[37] If we consider the use of dodecanthiol as reaction source and surface ligands, the large off-stoichiometry observed in Cu-rich $CuInS_2$ NCs may be partially due to the configuration with copper-occupied surface. This assumption is in accordance with the observed size-dependent [Cu]/[In] molar ratio of $CuInS_2$ NCs[14] and other reports on PbSe NCs.[55]

Samples with defined composition were further studied by X-ray diffraction (XRD) to analyze their structures. **Figure 1**a shows the XRD patterns of $CuInS_2$ NCs. Although there are very small amount of measurable secondary phase in some products, XRD pattern comparison suggests that the resulting samples may be of tetragonal phase (see Figure S2 in the Supporting Information). Three obvious diffraction peaks correspond to the (112), (220)/(204), and (312)/(116) planes of the tetragonal phase. The structure of these NCs was confirmed to be tetragonal phase by using Raman spectroscopy, the results of which are shown in Figure 1b. The appearance of a main peak at around 290 cm^{-1} corresponds to the A1 phonon model in the tetragonal structure of $CuInS_2$ crystals.[56] Except for the peak at around 290 cm^{-1}, the sample with [Cu]/[In] molar ratio of 2.9 has another peak at approximately 475 cm^{-1}, which relates to the CuS phase. It is not surprising to detect vibrational models of CuS in copper-rich NCs, which is a well-known phenomenon in bulk $CuInS_2$ material.[57]

In addition to the off-stoichiometry, I–III–VI materials also have structural anomalies relative to their II–VI analogs due to the existence of two cations as well as the bond alternation (bond lengths $R_{Cu\text{-}S} \neq R_{In\text{-}S}$). Since the structural parameters of ternary compounds play a significant role in elucidation of their optical band properties,[52,53] we here studied the unit cell parameters (a, c), tetragonal strain parameter (η), and anion displacement parameter (u) of as-prepared $CuInS_2$ NCs as a function of [Cu]/[In] molar ratio. The unit cell parameters (a, c) were calculated as[58]

$$d = \frac{a}{\sqrt{h^2 + k^2 + \frac{l^2}{(c/a)^2}}} \quad (1)$$

where d is the interplanar spacing, a and c are unit cell parameters, and, h, k, l are Miller indices.

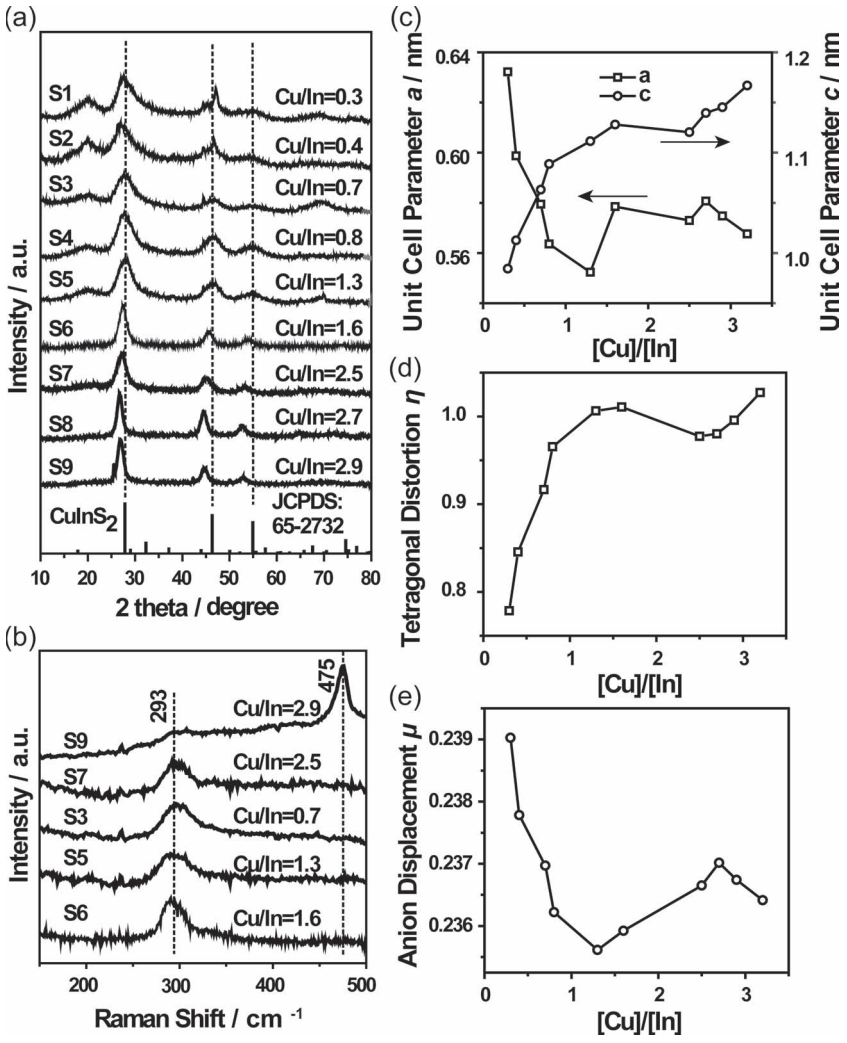

Figure 1. a) XRD patterns and b) Raman spectra of $CuInS_2$ NCs with different [Cu]/[In] molar ratios. c) Plots of unit cell parameters *a* and *c*. d) Tetragonal distorations and e) anion displacement parameters of the $CuInS_2$ NCs as a function of their [Cu]/[In] molar ratios.

Figure 1c shows the variation of structural parameters *a* and *c* with [Cu]/[In] molar ratio. For copper-rich samples, the *a* unit-cell parameter decreases with [Cu]/[In] molar ratio, while the *c* unit-cell parameter exhibits the contrary behavior. The tetragonal structure of I–III–VI ternary compounds can be considered as being derived from the zinc-blende structure. Because the bond length of In–S is about 5% larger than that of the Cu–S bond, the increase of the *a* unit-cell parameter may be due to the presence of In on Cu antisite defects, which is consistent with our assumption of the observed off-stoichiometry. The tetragonal strain parameter (η), defined as $\eta = c/2a$, provides the crystal distortion in comparison to the zinc-blende phase. The tetragonal strain parameter (η) varies from 0.778 to 1.027 for $CuInS_2$ NCs with different [Cu]/[In] molar ratio. This implies that the crystal structures of $CuInS_2$ NCs are distorted for the copper-deficient samples. For the copper-deficient samples, the tetragonal strain parameter (η) gradually decrees with decreasing [Cu]/[In] ratio, indicating that the tetragonal deformation becomes more obvious with increasing copper deficiency. The distortion deformation of approximately 22% of $CuInS_2$ NCs is larger than their bulk counterpart (at most, it is 12% for bulk materials).[53] This suggests that the Cu–S and In–S bond-length mismatch effects were enhanced in nanoscale materials. The amount of anions that displaced from the ideal tetrahedral site is defined as anion displacement parameter (u), which can be calculated as[51]

$$u = \frac{1}{4} + \alpha/a^2 \tag{2}$$

where $\alpha = R_{CuS}{}^2 - R_{InS}{}^2$; R_{CuS} and R_{InS} are cation-anion bond lengths.[52]

The values of displacements parameters for $CuInS_2$ NCs, varying from 0.235 to 0.239, are close to the reported value 0.236 of bulk materials. Like the bulk phase, bond alternation is also manifest for the NC system.

We also studied the off-stoichiometry effects on the optical properties of $CuInS_2$ NCs. **Figure 2**a shows the resulting $CuInS_2$ samples with different [Cu]/[In] molar ratio in toluene and corresponding picture under a UV lamp. Under UV 365 nm light excitation, the PL emission properties of these samples vary with their [Cu]/[In] molar ratio. With the naked eye, we are not able to observe light emissions in the products with [Cu]/[In] molar ratios of 2.5, 2.7, or 2.9 under UV radiation; the other samples, with [Cu]/[In] molar ratios of 1.6, 1.3, 0.8, 0.7, 0.4, and 0.3, are all red emissive without obvious difference. These samples were further studied by using UV-Vis absorption and PL spectra. Figure 2b shows that both of the absorption and emission spectra shifted to shorter wavelengths with decreasing [Cu]/[In] molar ratio. PL peaks shifted form around 760 to 650 nm, maintaining the FWHM of approximately 120 nm. The PL QYs of these samples were measured by comparing the integrated emission of the QDs samples in solution with that of a fluorescent dye following a published method.[59,60] The PL QYs of $CuInS_2$ NCs can be significantly influenced by their [Cu]/[In] molar ratio,with a maximum of around 11% for the sample with [Cu]/[In] molar ratio of 0.7. A schematic ternary (Cu–In–S) phase diagram is plotted to clarify the stoichiometry effects (see Figure 2c). It is clearly shown that most of the luminescent $CuInS_2$ samples locate in the copper deficient region and the sample with around 30% deficiency has an optimized PL QY. This observation is of profound significance and provides essential guidance for the highly luminescent $CuInS_2$ NCs.

In previous reports by us and others, the PL spectra of $CuInS_2$ NCs have been found to be excitation-intensity- and wavelength-dependent.[12,13] In this work, spectroscopic study indicates that the PL emission of $CuInS_2$ NCs is related to

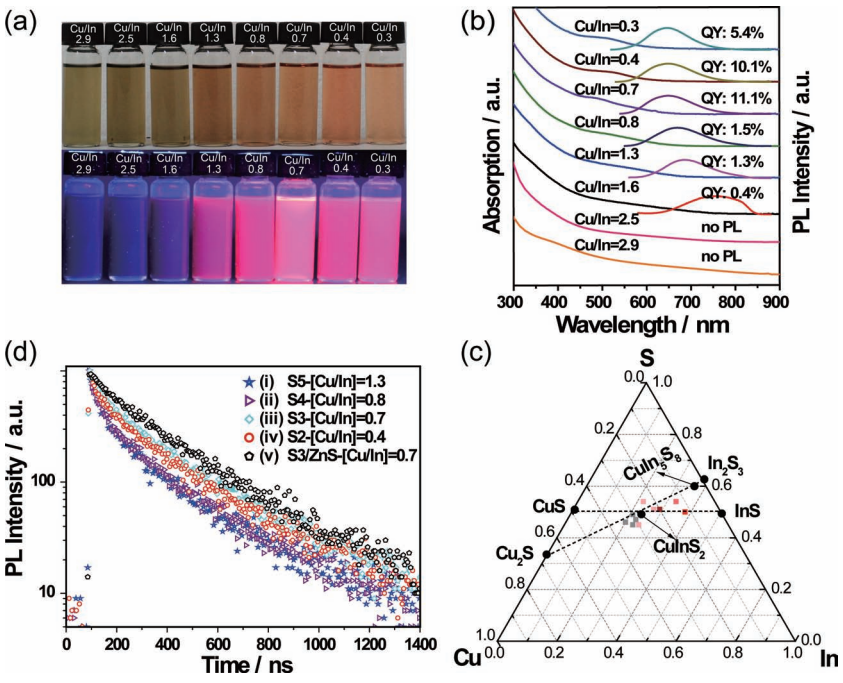

Figure 2. a) Photograph of the resulting $CuInS_2$ samples with different [Cu]/[In] molar ratio in toluene and corresponding picture under a UV lamp. b) Absorption and PL spectra of as-prepared $CuInS_2$ NCs with different [Cu]/[In] molar ratios. c) Schematic ternary (Cu–In–S) phase diagram (the samples with PL emissions are illustrated by painting squares various colors, with the depth of color representing the value of PL QYs). d) PL decays of $CuInS_2$ NCs with [Cu]/[In] molar ratio of 1.3 (i), 0.8 (ii), 0.7 (iii), 0.4 (iv), and $CuInS_2$/ZnS NCs (v).

copper deficiency. All of these results suggest a donor-acceptor-pair (DAP) recombination mechanism. The PL QYs of $CuInS_2$ NCs depend on the defect concentration. If the DAP states are formed by $2V_{Cu}^{-} + In_{Cu}^{2+}$ pairs. The PL QY was found to have a maximum value at a defect concentration of one defect pair per three units of $CuInS_2$. To further understand PL properties in $CuInS_2$ NCs, we studied the PL dynamics of $CuInS_2$ NCs. The time-resolved PL spectra of $CuInS_2$ NCs with different [Cu]/[In] molar ratio at their emission peak are shown in Figure 2d. The $CuInS_2$ NCs with [Cu]/[In] molar ratio of 0.7, having the highest PL QYs among the $CuInS_2$ cores, exhibit longer PL lifetime than the other samples. Based on these, a simple model, schematically described in **Figure 3**, was proposed to explain the PL properties of $CuInS_2$ NCs. The excitons generated by light absorption of $CuInS_2$ NCs transform to the DAP defect states

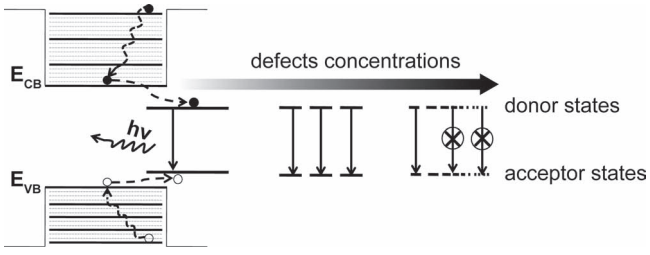

Figure 3. A schematic diagram used to demonstrate the PL properties of $CuInS_2$ NCs.

and recombine to give out emissions. The PL quenching of the samples with high concentration DAP defect states may be due to the interaction effects between DAP states.

To optimize the PL properties, we prepared $CuInS_2$-based core/shell NCs with PL emissions covering most of the visible window (ca. 500–750 nm) (**Figure 4**a,b) by incorporating Zn into $CuInS_2$ NCs with [Cu]/[In] molar ration of 0.7, as well as coating a ZnS shell layer. The obtained NCs can be purified and dried under inert conditions, producing high luminescence NC powders (Figure 4c). The obtained core/shell NCs have PL QYs of 40–65% for all samples (see the Supporting Information, Table S2). By simple scaling up the synthesis, this protocol can easily produce tens of grams of red emissive materials per batch experiment (Figure 4d). High-resolution transmission emission microscopy (HRTEM) images (Figure 4e) of the sample, obtained from the large amount synthesis, shows that the obtained NCs are high crystalline and have an average diameter of around 5 nm. Figure 4f shows the XRD patterns of the core/shell NCs with red (peak at 617 nm), yellow (peak at 553 nm), and green (peak at 527 nm) emissions, indicating the resulting NCs are of high quality.

Our preparation of high-quality $CuInS_2$-based NCs provides us an opportunity to explore the application of these materials in LEDs. The highly luminescent samples with emission peak at 606 and 577 nm were used to fabricate light-emitting devices. The structure of a typical ITO/hole transport layer (HTL)/NCs/electron transport layer (ETL)/Ca/Al was employed to fabricate QD-LEDs. Poly[*N*,*N*-bis(4-butylphenyl)-*N*,*N*-bis(phenyl)benzidine] (poly-TPD) and tris-(8-hydroxyquinoline) aluminium (Alq_3) were chosen as HTL and ETL layers, respectively. More details of the device fabrication and characterization are provided in the Experimental Section. The normalized EL spectra (square symbol lines) and their corresponding PL spectra (circular symbol lines) with maxima at 606 and 577 nm are shown in **Figure 5**a,d. The EL spectra have similar line shapes to the PL spectra, with some broadening compared to the PL plot, indicating that the device emissions are mainly due to the NCs. Figure 5b,e plot the measured luminance–current–voltage (*L*–*I*–*V*) characteristics of the LED devices with red and yellow colors. The luminous efficiency and power efficiency of the fabricated devices were calculated and are plotted in Figure 5c,f. The turn-on voltages (V_{on}), defined as the bias voltage applied to an LED producing a brightness of 10 cd m^{-2}, are approximately 4.8 V for red color devices and 5 V for yellow color devices. It is noteworth that the turn-on voltage of yellow devices is much lower than that of the $CuInS_2$/ZnSe/ZnS-based devices in our recent report. This implies that the barrier height for the charge injection of $CuInS_2$/ZnS is minimized compared to $CuInS_2$/ZnSe/ZnS multiple-shell NCs. The maximum luminance reached approximately 1700 cd m^{-2} (at 14 V) for red devices and around 2100 cd m^{-2} (at 15 V) for yellow devices.

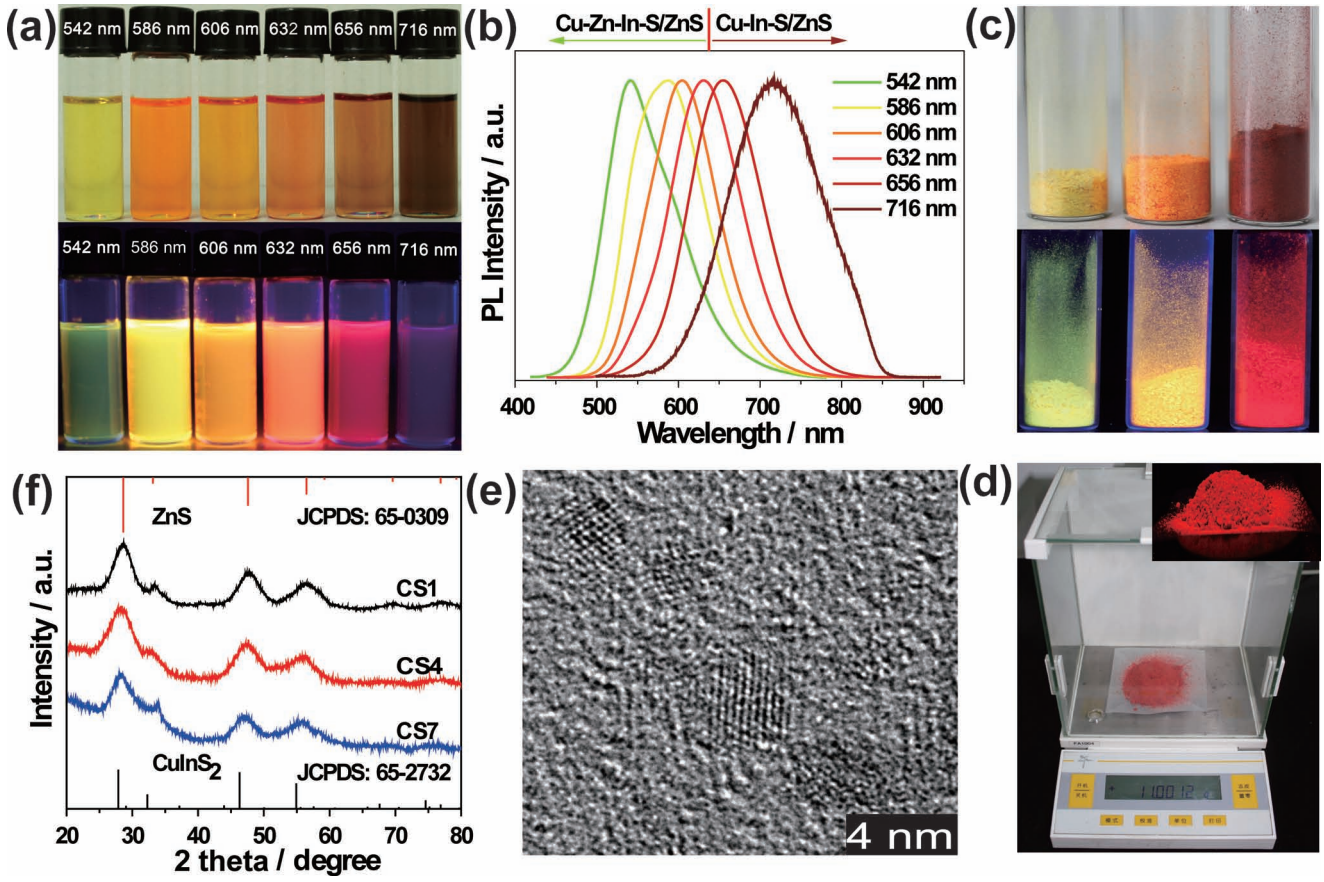

Figure 4. a) Optical image of $CuInS_2$/ZnS or ($CuInS_2$–ZnS)/ZnS NCs in toluene and corresponding picture under UV 365 nm excitation. b) PL spectra of as-prepared $CuInS_2$-based emissive NCs. c) The obtained NC powders with green, yellow, and red colours. d) Optical picture of the sample (around 11 g) obtained from large-scale synthesis, and the cooresponging picture under UV excitation (inset). e) HRTEM image of the sample obtained from large-scale synthesis. f) XRD patterns of core/shell NCs with red (peak at 617 nm), yellow (peak at 553 nm), and green (peak at 527 nm) emissions.

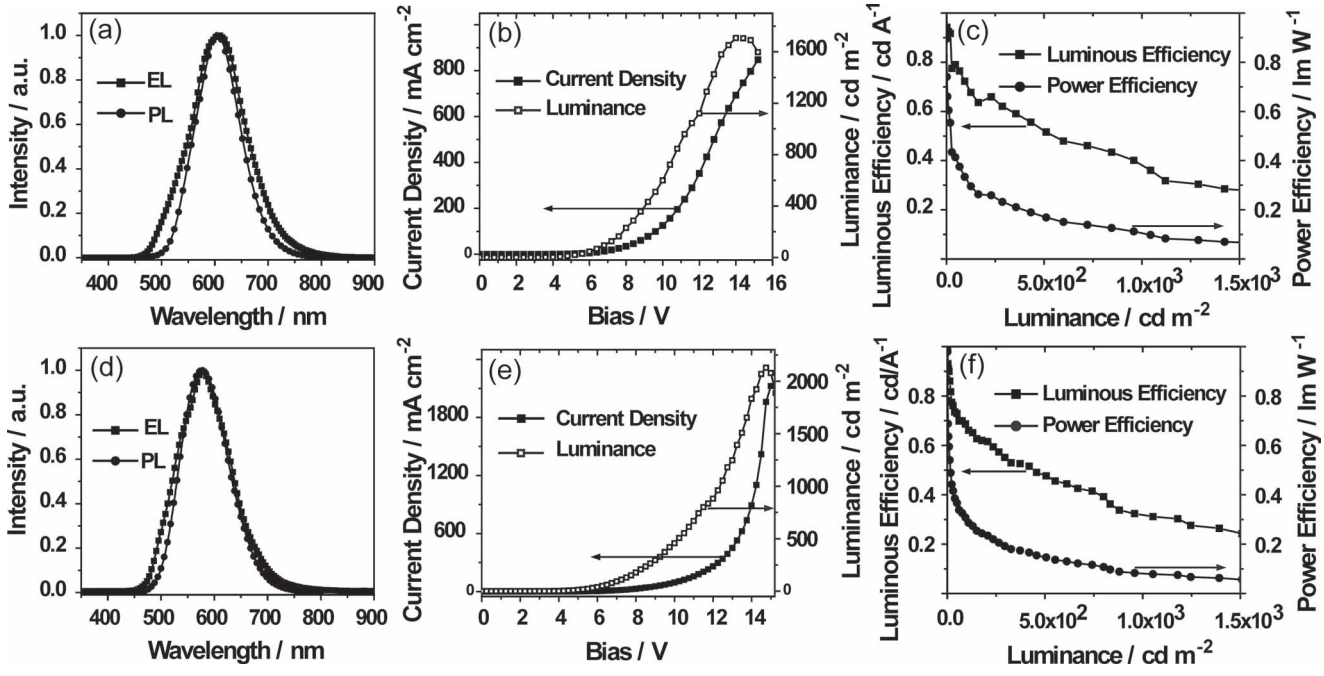

Figure 5. a,d) The PL spectra and corresponding EL of two selected $CuInS_2$ based core/shell samples with PL emission peak at 606 and 577 nm. b,e) Current density and luminance of the devices with red and yellow emission colors as a function of applied bias. c,f) Current efficiency and power efficiency of red and yellow devices as a function of current density.

A luminous efficiency of 0.92 cd A^{-1} and a power efficiency of 0.61 lm W^{-1}, at an injection current density of 1.18 mA cm^{-2}, corresponding to a brightness of 10 cd m^{-2}, were observed for red devices. For the yellow devices, the luminous efficiency was 0.88 cd A^{-1} and power efficiency 0.58 lm W^{-1}, at an injection current density of 1.03 mA cm^{-2}, corresponding to a brightness of 10 cd m^{-2}. At standard display brightness (100–500 cd m^{-2}), the red device shows moderate luminous efficiency of 0.70 at 100 cd m^{-2}, changing to 0.52 at 500 cd m^{-2}; and, the yellow device a luminous efficiency of 0.65 at 100 cd m^{-2}, changing to 0.47 at 500 cd m^{-2}. The power conversion efficiency reached a maxima at near turn-on and then decreased to 0.32 and 0.29 lm W^{-1} (at 100 cd m^{-2}) for the red and yellow devices, respectively. The device performance of our samples is much better than our recent report,[47] indicating that the as-prepared materials in this work are of high quality.

3. Conclusions

This work has demonstrated off-stoichiometry effects on the crystal structure and optical properties of $CuInS_2$ NCs utilizing a simple model adapted from the bulk materials. Although the model for $CuInS_2$ NCs should be further developed, it can explain the observed structural and PL emission evolutions with the [Cu]/[In] molar ratio. Importantly, we are able to synthesize highly emissive and color-tunable colloidal $CuInS_2$-based NC powder at tens of grams scale by choosing a suitable [Cu]/[In] molar ratio, adapting the alloying and shell-coating strategies. The synthetic method is simple, hassle-free, and can be scaled to produce tens of grams without hindering the quality of NCs. The as-prepared highly luminescent NCs are high quality with superior emission properties in the wavelength range 500 to 800 nm. We examined the performance of these samples in EL devices. The performance of light-emitting devices is much better than the previous reports. The observed maximum luminance is approximately 1700 cd m^{-2} (at 14 V) for the red devices with emission peak at 606 nm, and approximately 2100 cd m^{-2} (at 15 V) for the yellow devices with emission peak at 577 nm. The current efficiency is nearly two times higher than that previously reported.[47] The availability of gram-scale highly emissive and color-tunable $CuInS_2$-based NCs opens the door to explore their applications as in vivo biomarkers, phosphors, and labels in other fields.

4. Experimental Section

Materials: Copper(I) iodide (CuI, Alfa Aesar, 98%), indium(III) acetate ($In(OAc)_3$, Alfa Aesar, 99.99%), zinc acetate dehydrate ($Zn(OAc)_2$, Alfa Aesar, ≥97%), zinc stearate ($Zn(St)_2$, Xilong chemical corporation, 84.6%), 1-dodecanethiol (DDT, Alfa Aesar, 98%), 1-octadecene (ODE, Alfa Aesar, 90%), oleic acid (OA, Alfa Aesar, 90%), oleylamine (OLA, J&K Scientific, 90%), Rhodamine B (RhB, Aldrich), poly[*N*,*N*-bis(4-butylphenyl)-*N*,*N*-bis(phenyl)benzidine] (poly-TPD), tris-(8-hydroxyquinoline) aluminium (Alq_3) were used without further purification.

Synthesis of $CuInS_2$ NCs: In a typical synthetic procedure of $CuInS_2$ NCs with [Cu]/[In] molar ratios of 0.7, CuI (0.076 g, 0.4 mmol) and $In(OAc)_3$ (0.464 g, 1.6 mmol) were mixed with dodecanethiol (1 mL) in a 50 mL three-necked flask, which was followed by the addition of ODE (10 mL). The reaction mixture was degassed under vacuum for 20 min at 120 °C. Next, oleic acid (0.5 mL) was added into the reaction flask, and the solution was continuously degassed for 20 min, then purged with nitrogen for 20 min. Subsequently, the solution was heated to 210 °C for 60 min under nitrogen flow until a deep red colloidal solution was formed. Afterward, the reaction solution was cooled to room temperature and precipitated by adding excess acetone. The flocculent precipitate was centrifuged at 8500 rpm for 5 min and the supernatant decanted. This process was repeated a minimum of three times and the precipitation was then dispersed in a nonpolar solvent (toluene, chloroform) or dried to powder for characterization.

$CuInS_2$ NCs with [Cu]/[In] molar ratios of 0.3, 0.4, 0.7, 0.8, 1.3, 1.6, 2.5, 2.7, and 2.9 were synthesized by varying the raw materials ratio.

Synthesis of ($CuInS_2$-ZnS)/ZnS NCs: Zinc stock solution was first prepared as follows. $Zn(OAc)_2$ (0.528g, 3 mmol), OLA (2 mL), and ODE (2 mL) were added to a 50 mL three-necked flask. The solution was degassed for 30 min and purged with nitrogen for 30 min. Next, the solution was heated to 130 °C under nitrogen flow until a clear colorless solution was formed. The obtained Zn stock solution was maintained at this stage for following injection. For a typical synthetic reaction of ($CuInS_2$-ZnS)/ZnS NCs with yellow emission (peak at 586 nm), CuI (0.038 g, 0.2 mmol), $Zn(OAc)_2$ (0.088 g, 0.5 mmol) and $In(OAc)_3$ (0.232 g, 0.8 mmol) were mixed with dodecanethiol (2 mL) and ODE (4 mL) in a 50 mL three-necked flask. The reaction mixture was degassed under vacuum for 20 min at 120 °C. After that, oleic acid (1 mL) was added into the reaction flask, and the solution was continuously degassed for another 20 min, followed by purging with nitrogen for 20 min. The solution was then heated to 230 °C for 30 min under nitrogen flow until a colloidal solution was formed. Subsequently, Zn stock solution (4 mL) was added dropwise into the reaction mixture. The washing process was the same as that described for $CuInS_2$ NCs. The precipitates were dried under vacuum for 1 h at 50 °C to get NC powders. ($CuInS_2$-ZnS)/ZnS NCs with emissions from 520 to 610 nm were prepared by varying the fraction of zinc in the core precursor mixture from 0% to 50%.

Characterization: Absorption spectra were recorded on a V-570 UV-Vis spectrophotometer. PL spectra were taken using a FP-6600 luminescence spectrometer. The PL QYs of samples were measured by using rhodamine B as a standard reference (rhodamine B dissolved in ethanol, QY: 97%) and comparing integrated PL intensities using the standard procedure.[59,60] The PL emission of rhodamine B was measured with excitation wavelength at 520 nm. The QYs of $CuInS_2$ NCs calculated as

$$QY = QY_R \times \frac{I}{I_R} \times \frac{A_R}{A} \times \frac{n^2}{n_R^2} \quad (3)$$

where QY is the quantum yield, I is the measured integrated PL emission intensity, n is refractive index (n = 1.497 for toluene; n = 1.362 for ethanol) and A is the optical density at the excitation wavelength (A is typically around 0.05). The subscript R refers to the parameters of the reference. All the $CuInS_2$ NC samples were measured using FP-6600 spectrophotometer with excitation wavelength at 500 nm. HRTEM images were taken on a JEM-2100F transmission electron microscope with an acceleration voltage of 200 kV. XRD measurements were carried out on a Rigaku D/max-2500 X-ray diffractometer with graphite monochromated Cu Kα radiation (λ = 1.5418 Å) with a scanning rate of 1 degree min^{-1}. The Raman spectra were recorded by using Horiba Jobin-Yoon T6400 Raman spectrometer.

Device Fabrication: All the devices were fabricated on commercially line-patterned indium tin oxide (ITO) coated glass having a sheet resistance of 10 Ω sq^{-1}. The width of the ITO lines is 2 micrometer. Substrates were ultrasonically cleaned with a standard regimen of detergent, acetone, and isopropyl alcohol for 15 min each, followed by UV ozone treatment for 15 min. PEDOT:PSS (Baytron-P, Bayer AG) was spin-coated onto a UV-ozone treated ITO substrate and then dried at 150 °C in a vacuum oven for 15 min. Poly-TPD in 1,2-dichlorobenzene (20 mg mL^{-1}) was spin-coated on the top of the PEDOT at 2000 rpm for 60 s in the glove box. The polymer layers were dried for over 30 min at approximately 150 °C in the glove box. QD dispersions in toluene were then spin coated

at 2000 rpm for 60 s on top of the poly-TPD. After a subsequent drying for 15 min at around 80 °C in the glove box, the samples were transferred to a vacuum chamber and a 30 nm thick Alq_3 layer was thermally deposited with base pressure of 3×10^{-4} Pa. After that, a 10 nm Ca and 100 nm thick Al cathode was deposited using a shadow mask with 2 mm width. The active area of the devices was thus 4 mm^2. Film thicknesses were monitored using a calibrated quartz crystal microbalance (QCM). The current–luminance–voltage (*I–L–V*) characteristics were measured using a computer-controlled Keithley 236 SMU and Keithley 200 multimeter coupled with a calibrated Si photodiode. EL spectra were measured by an Ocean Optics 2000 spectrometer, which couples a linear charge coupled device (CCD)-array detector ranging from 350 to 1100 nm.

Supporting Information

Supporting Information is available from the Wiley Online Library or from the author.

Acknowledgements

This research was supported under the National Basic Research Program of China (No. 2011CB933600), NSFC Research Grants (No. 51003005 and 91023039), Excellent Young Scholars Research Fund of Beijing Institute of Technology (No.2010Y0913), Beijing NOVA Program (No. 2010B038) and the 111 research base (BIT111-201101).

Received: October 17, 2011
Revised: January 19, 2012
Published online: March 2, 2012

[1] G. D. Scholes, *Adv. Funct. Mater.* **2008**, *18*, 1157.
[2] V. L. Colvin, M. C. Schlamp, A. P. Alivisatos, *Nature* **1994**, *370*, 354.
[3] Q. J. Sun, Y. A. Wang, L. S. Li, D. Y. Wang, T. Zhu, J. Xu, C. H. Yang, Y. F. Li, *Nat. Photonics* **2007**, *1*, 717.
[4] W. C. W. Chan, S. M. Nie, *Science* **1998**, *281*, 2016.
[5] L. Basabe-Desmonts, D. N. Reinhoudt, M. Crego-Calama, *Chem. Soc. Rev.* **2007**, *36*, 993.
[6] W. U. Huynh, J. J. Dittmer, A. P. Alivisatos, *Science* **2002**, *295*, 2425.
[7] J. Tang E. H. Sargent, *Adv. Mater.* **2011**, *23*, 12.
[8] J. He, H. Z. Zhong, G. D. Scholes, *Phys. Rev. Lett.* **2010**, *105*, 046601.
[9] D. V. Talapin, J. S. Lee, M. V. Kovalenko, E. V. Shevchenko, *Chem. Rev.* **2010**, *110*, 389.
[10] H. Z. Zhong, T. Mirkovic, G. D. Scholes, *Comprehensive Nanoscience and Technology Vol. 5: Nanocrystal Synthesis*, (Eds: D. Andrews, G. Scholes, G. Wiederrecht), Elsevier **2010**, p. 153–201.
[11] T. Omata, K. Nose, S. Otsuka-Yao-Matsuo, *J. Appl. Phys.* **2009**, *105*, 073106.
[12] S. L. Castro, S. G. Bailey, R. P. Raffaelle, K. K. Banger, A. F. Hepp, *J. Phys. Chem. B* **2004**, *108*, 12429.
[13] H. Z. Zhong, Y. Zhou, M. F. Ye, Y. J. He, J. P. Ye, C. He, C. H. Yang, Y. F. Li, *Chem. Mater.* **2008**, *20*, 6434.
[14] H. Z. Zhong, S. S. Lo, T. Mirkovic, Y. C. Li, Y. Q. Ding, Y. F. Li, G. D. Scholes, *ACS Nano* **2010**, *4*, 5253.
[15] H. Nakamura, W. Kato, M. Uehara, K. Nose, T. Omata, S. Otsuka-Yao-Matsuo, M. Miyazaki, H. Maeda, *Chem. Mater.* **2006**, *18*, 3330.
[16] D. C. Pan, L. J. An, Z. M. Sun, W. Hou, Y. Yang, Z. Z. Yang, Y. F. Lu, *J. Am. Chem. Soc.* **2008**, *130*, 5620.
[17] R. G. Xie, M. Rutherford, X. G. Peng, *J. Am. Chem. Soc.* **2009**, *131*, 5691.
[18] L. Li, T. J. Daou, I. Texier, T. T. K. Chi, N. Q. Liem, P. Reiss, *Chem. Mater.* **2009**, *21*, 2422.
[19] Q. J. Guo, S. J. Kim, M. Kar, W. N. Shafarman, R. W. Birkmire, E. A. Stach, R. Agrawal, H. W. Hillhouse, *Nano Lett.* **2008**, *8*, 2982.
[20] M. G. Panthani, V. Akhavan, B. Goodfellow, J. P. Schmidtke, L. Dunn, A. Dodabalapur, P. F. Barbara, B. A. Korgel, *J. Am. Chem. Soc.* **2008**, *130*, 16770.
[21] M. E. Norako, M. A. Franzman, R. L. Brutchey, *Chem. Mater.* **2009**, *21*, 4299.
[22] J. Tang, S. Hinds, S. O. Kelley, E. H. Sargent, *Chem. Mater.* **2008**, *20*, 6906.
[23] B. Koo, R. N. Patel, B. A. Korgel, *J. Am. Chem. Soc.* **2009**, *131*, 3134.
[24] W. M. Du, X. F. Qian, J. Yin, Q. Gong, *Chem. Eur. J.* **2007**, *13*, 8840.
[25] D. S. Wang, W. Zheng, C. H. Hao, Q. Peng, Y. D. Li, *Chem. Commun.* **2008**, 2556.
[26] C. Sun, J. S. Gardner, E. Shurdha, K. R. Margulieux, R. D. Westover, L. Lau, G. Long, C. Bajracharya, C. M. Wang, A. Thurber, A. Punnoose, R. G. Rodriguez, J. J. Pak, *J. Nanomater.* **2009**, 748567.
[27] T. Toromoto, S. Ogawa, T. Adachi, T. Kameyama, K. Okazaki, T. Shibayama, A. Kuno, S. Kuwabata, *Chem. Commun.* **2011**, *46*, 2082.
[28] X. S. Tang, W. L. Cheng, E. S. G. Choo, J. M. Xue, *Chem. Commun.* **2011**, *47*, 5217.
[29] X. S. Tang, K. Yu, Q. Xu, E. S. G. Choo, G. K. L. Goh, J. M. Xue, *J. Mater. Chem.* **2011**, *21*, 11239.
[30] L. Li, A. Pandey, D. J. Werder, B. P. Khanal, J. M. Pietryga, V. I. Klimov, *J. Am. Chem. Soc.* **2011**, *133*, 1176.
[31] W. J. Zhang, X. H. Zhong, *Inorg. Chem.* **2011**, *50*, 4065.
[32] J. Feng, M. Sun, F. Yang, X. R. Yang, *Chem. Commun.* **2011**, *47*, 6422.
[33] J. Zhang, R. G. Xie, W. S. Yang, *Chem. Mater.* **2011**, *23*, 3357.
[34] H. Z. Zhong, Z. B. Wang, E. Bovero, Z. H. Lu, F. C. J. M. van Veggel, G. D. Scholes, *J. Phys. Chem. C* **2011**, *115*, 12396.
[35] S. Sarkar, N. S. Karan, N. Pradhan, *Angew. Chem. Int. Ed.* **2011**, *50*, 6065.
[36] Y. Hamanaka, T. Kuzuya, T. Sofue, T. Kino, K. Ito, K. Sumiyama, *Chem. Phys. Lett.* **2008**, *466*, 176.
[37] S. B. Zhang, S. H. Wei, A. Zunger, H. Katayama-Yoshida, *Phys. Rev. B* **1998**, *57*, 9642.
[38] G. Dagan, F. Abou-Elfotouh, D. J. Dunlavy, R. J. Matson, D. Cahen, *Chem. Mater.* **1990**, *2*, 286.
[39] M. Uehara, K. Watanabe, Y. Tajiri, H. Nakamura, H. Maeda, *J. Chem. Phys.* **2008**, *129*, 134709.
[40] T. Erdem, H. V. Demir, *Nat. Photonics* **2011**, *5*, 126.
[41] L. Qian, Y. Zhang, J. G. Xue, P. H. Holloway, *Nat. Photonics* **2011**, *5*, 543.
[42] P. O. Anikeeva, J. E. Halpert, M. G. Bawendi, V. Bulovic, *Nano Lett.* **2009**, *9*, 2532.
[43] A. L. Rogach, N. Gaponik, J. M. Lupton, C. Bertoni, D. E. Gallardo, S. Dunn, N. L. Pira, M. Paderi, P. Repetto, S. G. Romanov, C. O'Dwyer, C. M. S. Torres, A. Eychmueller, *Angew. Chem. Int. Ed.* **2008**, *47*, 6538.
[44] N. Gaponik, S. G. Hickey, D. Dorfs, A. L. Rogach, A. Eychmueller, *Small* **2010**, *6*, 1364.
[45] Q. Q. Dai, C. E. Duty, M. Z. Hu, *Small* **2010**, *6*, 1577.
[46] Y. Zhang, C. Xie, H. P. Su, J. Liu, S. Pickering, Y. Q. Wang, W. W. Yu, J. K. Wang, Y. D. Wang, J. Hahm, N. Dellas, S. E. Mohney, J. Xu, *Nano Lett.* **2011**, *11*, 329.
[47] Z. A. Tan, Y. Zhang, C. Xie, H. P. Su, J. Liu, C. F. Zhang, N. Dellas, S. E. Mohney, Y. Q. Wang, J. K. Wang, J. Xu, *Adv. Mater.* **2011**, *23*, 3553.
[48] H. Kim, J. Y. Han, D. S. Kang, S. W. Kim, D. S. Jang, M. Suh, A. Kirakosyan, D. Y. Jeon, *J. Crystal Growth* **2011**, *326*, 90.
[49] D. P. Puzzo, E. J. Henderson, M. G. Helander, Z. B. Wang, G. A. Ozin, Z. H. Lu, *Nano Lett.* **2011**, *11*, 1585.

[50] J. L. Lim, W. K. Bae, D. G. Lee, M. K. Nam, J. Y. Jung, C. H. Lee, K. H. Char, S. H. Lee, *Chem. Mater.* **2011**, *23*, 4459.
[51] J. E. Jaffe, A. Zunger, *Phys. Rev. B* **1983**, *27*, 5176.
[52] J. E. Jaffe, A. Zunger, *Phys. Rev. B* **1983**, *28*, 5822.
[53] J. E. Jaffe, A. Zunger, *Phys. Rev. B* **1984**, *29*, 1882.
[54] A. Zunger, *Int. J. Quantum Chem.* **1985**, *19*, 629.
[55] V. Petkov, I. Moreels, Z. Hens, Y. Ren, *Phys. Rev. B* **2010**, *81*, 241304.
[56] W. H. Koschel, M. Bettini, *Phys. Status Solidi B* **1975**, *72*, 729.
[57] M. Ishii, K. Shibata, H. Nozaki, *J. Solid. State. Chem.* **1993**, *105*, 504.
[58] A. R. West, *Solid State and Its Application*, John Wiley & Sons, Ltd., Aberdeen **1985**, Ch. 5.
[59] J. R. Lakowicz, *Principles of Fluorescence Spectroscopy*, 3rd Edition, Springer, New York **2006**, Ch 2.
[60] J. N. Demas, G. A. Crosby, *J. Phys. Chem.* **1971**, *75*, 991.